# Implications of volume loss on the seismic response of tunnels in coarse-grained soils

Kampas, G., Knappett, J.A., Brown, M.J., Anastasopoulos, I., Nikitas, N., Fuentes, R.

**Abstract**

This paper examines the seismic response of a "horseshoe–shaped" tunnel, inspired from a recently constructed Metro tunnel in Santiago, Chile. A FE analysis is conducted, investigating the effect of soil density, apparent cohesion, the interface between the tunnel and the surrounding soil, the intensity of the seismic excitation and the effect of volume loss due to tunnel construction on the seismic behaviour of tunnels. The presence of apparent cohesion leads to a reduction of tunnel distress and to smaller post-earthquake ground settlements over a reduced distance from the tunnel. The consideration of volume loss does not significantly affect the acceleration field around the tunnel, but does beneficially decrease the lining forces. Furthermore, although it leads to an increase of the pre-earthquake settlements, it is found to decrease the co-seismic settlements. Finally, it was found that the most conservative model regarding the design detailing of the tunnel lining would be considering a rough interface, zero cohesion, and negligible volume loss (i.e., an ideally-excavated tunnel).

## 1. INTRODUCTION

Underground structures, such as tunnels, typically constitute critical infrastructure whose serviceability needs to be maintained after major earthquakes. However, fully understanding their seismic behaviour is challenging due to the large number of parameters involved, including those associated with the soil, the tunnel structure, and their interface. In general, tunnels are less sensitive to seismic loading compared to above-ground structures. This insensitivity of tunnels is largely due to their negligible mass compared to the soil, due to which the generated inertia forces are far less important than the kinematic loading exerted from their interaction with the surrounding soil [e.g., Dowding & Rozen 1978; Wang 1993; Kawashima 2000; Anastasopoulos & Gazetas 2010; Yu et al. 2013; Tsinidis et al. 2016; Yu et al. 2018; Yu et al. 2019].

However, some notable case histories in relatively recent earthquake have proven that under certain conditions tunnels may experience severe damage or even collapse due to strong seismic shaking. These include the collapse of the Daikai metro station during the notorious 1995 Kobe earthquake [Iida et al. 1996; Nakamura et al. 1996], of several "horseshoe"–shaped tunnels in Taiwan during the 1999 Chi-Chi

earthquake [Ueng et al. 2001], and of the Bolu tunnel in during the 1999 Kocaeli earthquake in Turkey [O'Rourke et al. 2001; Anastasopoulos & Gazetas 2010; Hashash 2011; Kontoe et al. 2011].

The seismic response of tunnels has been investigated numerically and experimentally, by centrifuge model and shake-table testing, but the focus has mainly been on circular or square tunnel sections [e.g., Anastasopoulos et al. 2007; 2008; Amorosi & Boldini 2009; Anastasopoulos & Gazetas 2010; Cilingir & Madabushi 2011; Kontoe et al. 2011; Lanzano et al. 2015; Tsinidis et al. 2016a; 2016b; Yuan et al. 2018; Yu et al. 2018; Zhang et al. 2019a, b]. Most importantly, previous research on the subject has focussed on wished-in-place tunnel linings, ignoring the effects of the construction sequence, except some isolated studies [see Kontoe et al. 2008]. Another important effect of tunnelling is the ground surface settlements during tunnel excavation, which are a function of stress relief and volume loss. Several previous studies have dealt with tunnelling-induced ground settlements [e.g., Aoyagi, 1985; Bloodworth 2002; Dimmock & Mair, 2007; Dragojevic, 2012; Marshall et al., 2012; Zhou et al., 2014; Zhou, 2015; Avgerinos et al., 2016], but to the best of our knowledge, the implications of initial stress relief and volume loss on the seismic response of tunnels has not been systematically addressed. The initial deformations due to tunnel construction lead to a different initial strain (and stress) field within the surrounding soil, which may affect the seismic response of the tunnel. The collapse of the Bolu tunnel was largely due to such effects.

Therefore, the main scope of this paper is to address the effects of volume loss due to tunnel construction on the subsequent seismic performance of the tunnel and of the surrounding ground. A "horseshoe"-shaped tunnel is considered, inspired by sprayed-concrete (NATM) Metro tunnels in coarse-grained soils in Santiago, Chile, which have recently been constructed. A series of numerical analyses are conducted employing the finite element (FE) method, in order to derive insights on the factors controlling the seismic response. The analyses are conducted employing an advanced soil constitutive model that accounts for both nonlinear pre-yielding behaviour and post-yielding isotropic hardening, and which has been thoroughly validated against centrifuge model test results for a range of seismic soil-structure interaction problems on non-liquefiable sand, including slopes [Al-Defae et al., 2013], above-ground structures [Knappett et al.,

2015], and tunnels [Lanzano et al., 2015]. The investigated parameters include: (a) soil properties, covering a wide range of stiffness and strength parameters for dense (non-liquefiable) coarse-grained deposits; (b) apparent cohesion due to a cohesive matrix material (e.g., fine plastic silts occurring alongside larger particles in historic river deposits, which are characteristic of local site conditions in Santiago); (c) the properties of the soil–tunnel interface; (d) the intensity of the seismic excitation; and – most importantly – (e) the effect of volume loss due to tunnel construction.

## 2. FINITE ELEMENT MODELLING

### *2.1. Model description*

The numerical study is conducted using PLAXIS 2D 2016 and the developed plane-strain FE model is depicted in Fig. 1. The depth of the soil layer is 7 times the tunnel's height, $z = 56.6m \approx 7H_{tunnel}$ based on the stratigraphy of the profile, while, in order to minimise undesired boundary effects [Amorosi & Boldini 2009; Amorosi et al. 2010], the width of the model is approximately 40 times the tunnel's width, $W_{\mathrm{mod}\,el} = 430\,m \approx 40 \times W_{tunnel}$. The cover depth of the tunnel is $C \approx 2.25 H_{tunnel} = 18m$. The tunnel geometry is based on typical tunnel cross-sections encountered in the recently completed Line 3 of the Santiago Metro, which was under construction at the time the analyses were conducted. As shown in Fig. 1, the FE mesh has three zones of different local refinement, following the results of an initial sensitivity study using the reference ground motions (described later). The lateral boundaries of the model are viscous [Lysmer & Kuhlmeyer, 1969] with relaxation coefficients $C_1 = 1$ and $C_2 = 0.25$ along the horizontal and the vertical direction, respectively. Such viscous boundaries are commonly used in dynamic analyses, as they allow adequate absorption of laterally propagating seismic waves along both directions. However, in recent papers tied-node lateral boundaries have been used [Amorosi et al. 2017] as a more effective modelling technique. Therefore, a comparison between the absorbent viscous and tied-node lateral boundaries is presented in the Appendix in terms of horizontal displacement, acceleration and settlements

at the surface above the tunnel crown. The comparison did not reveal critical differences between the two lateral-boundary modelling approaches. The boundary conditions at the base of the model are fixed creating a high impedance contrast simulating the bedrock.

Damping constitutes a key parameter that can dominate seismic behaviour. Many publications have highlighted its effect on the dynamic response of soils [e.g., Zerwer et al. 2002; Kwok et al. 2007; Kontoe at al. 2011]. In this study, two types of damping are considered: (a) hysteretic damping due to nonlinear soil response, as described in the following section; and (b) frequency-dependent Rayleigh damping:

$$[C] = c_m[M] + c_k[K] \tag{1}$$

where: $[C]$ is the damping coefficient matrix; and $[M]$ and $[K]$ the mass and stiffness matrices, respectively. The Rayleigh coefficients are set to $c_m = 0.0005$ and $c_k = 0.005$, following the results of a series of centrifuge model tests [Al-Defae et al., 2013]. The selected coefficients result in predominantly stiffness-proportional Rayleigh damping, which effectively removes high frequency noise without leading to overdamping of the lower frequency parts of the response (which are the prime components of earthquake ground motions). This small extra Rayleigh damping is additional to the inherent numerical damping of the Newmark's time integration scheme.

### *2.2. Soil profile and constitutive modelling*

Soil behaviour is modelled using the "Hardening Soil model with small-strain stiffness" [Schanz et al. 1999; Benz 2006]: a nonlinear constitutive model with isotropic hardening, which is readily available in PLAXIS. The pre-yield part of the model follows a nonlinear relationship between the shear modulus, $G$, and the shear strain, $\gamma_s$, as proposed by Hardin & Drnevich [1972] and later modified by Santos &Correia [2001]:

$$\frac{G}{G_0} = \frac{1}{1 + 0.385\left|\frac{\gamma_s}{\gamma_{s,0.7}}\right|} \tag{2}$$

here: $G_0$ is the small-strain shear modulus and $\gamma_{s,0.7}$ is the shear strain that corresponds to $G/G_0 = 0.722$ . Plasticity is introduced as a cap-type yield surface, combined with a Mohr-Coulomb failure criterion [Smith & Griffiths 1982].

Since the present study focuses on coarse-grained soils, material properties representative of HST95 sand [Lauder et al., 2013; Bransby et al., 2011; Al-Defae et al., 2013] are considered, which has been shown to be representative of other granular materials [e.g., Knappett et al. 2017]. Two different relative densities $D_r = 60\%$ and $100\,\%$ are considered, offering range of peak friction angles representative of soil conditions in Metro Line 3. Along with $G$ and $\gamma_s$, the constitutive model also accounts for the variation of $G_0$ with depth $z$:

$$\frac{G_0}{G_0^{ref}} = \left( \frac{c'\cos\varphi' - \sigma_3' \sin\varphi'}{c'\cos\varphi' + p_{ref}\sin\varphi'} \right)^m \tag{3}$$

where: $G_0^{ref}$ is the shear modulus corresponding to the very small strain range at the reference stress of $p_{ref} = 100kPa$, $c'$ is the apparent cohesion, $\varphi'$ is the soil friction angle, $\sigma_3'$ is the effective confining stress, and $m$ is an empirical parameter controlling the shape of the relationship. The constitutive model requires eleven input parameters: unit weights under saturated and dry conditions, $\gamma_{sat}$, $\gamma_d$; six stiffness parameters (which are all stress-dependent): the secant stiffness in drained triaxial tests, $E_{50}$, the tangent stiffness for primary oedometer loading, $E_{oed}$, the unloading-reloading stiffness from drained triaxial tests, $E_{ur}$, the small-strain stiffness, $G_0^{ref}$, and the shear strain corresponding to $G/G_0 = 0.722$, $\gamma_{s,0.7}$, and one empirical parameter, $m$, controlling the variation of shear stiffness with confining stress as shown in Eq. (3); three strength parameters: $c'$, $\varphi'$, $\psi$, apparent cohesion, friction, and dilation angles, respectively. Table 1 summarizes the model parameters for the HST95 sand (for the two relative densities considered), according to the relationships proposed by Al-Defae et al. [2013]. However, this paper also considers soils

that may have granular particles in a cohesive matrix, adding some true cohesion (up to $c'$ = 50 kPa inspired by the soil profile in Santiago). A typical conservative assumption may be to such $c'$ in design; the implications of such an assumption are explored herein. Figure 2 presents the distribution of $G_0$ with depth $z$ for three different cases: (a) $D_r = 100\%; c' = 0kPa$, (b) $D_r = 60\%; c' = 0kPa$, and (c) $D_r = 60\%; c' = 50kPa$. The soil is considered to be normally consolidated, such that the initial value of the coefficient of earth pressure at rest is given by $K_0 = 1 - \sin \phi'$.

Kontoe at al. [2011] have used similar sophisticated kinematic hardening constitutive soil models, representing clayey soils, to assess the seismic response of circular cross-section tunnels. Similarly, Tsinidis et al. [2015; 2016a; 2016b] applied nonlinear elastoplastic constitutive models, representing dry sands, to investigate the seismic behaviour of square cross-section tunnels in sand, validating their numerical analysis results against centrifuge model tests. Based on the local site conditions of Santiago Metro Line 3, the ground water table is assumed to be well below the tunnel's invert, and therefore there is no liquefaction potential.

This constitutive model has been previously validated against centrifuge tests of linear elastic tunnel models in sand [Bilotta et al. 2014; Amorosi et al. 2014]. The ability of this model to produce ground motion amplification in the free-field has been previously demonstrated against centrifuge tests in Knappett et al. [2015].

### *2.3. Tunnel section*

As shown in Fig. 3, a reinforced concrete "horseshoe" tunnel section is considered, which is representative of a modern Metro tunnel development in Chile. The upper part of the tunnel section is circular, with a constant radius $R = 5.35m$ (arch section), intersecting at the bottom with a typical beam (flat section). The

tunnel lining is modelled with linear elastic plate elements, assuming the un-cracked stiffness with $EI_{arch} = 91{,}980 kNm^2$ and $EI_{flat} = 57{,}920 kNm^2$ for the arch and the flat sections, respectively.

### *2.4. Ground motions*

The scope of the present paper is not to conduct a specific case study on the basis of the local seismicity of Santiago, Chile. The main focus is to explore tunnel seismic response for seismic shaking ranging from moderate to severe. Within this context, the Takarazuka(000) record from the 1995 $M_w = 6.9$ Kobe earthquake (Fig. 4a) is used as seismic excitations, scaled to $a_g = 0.20g$, $0.45g$ and $0.69g$ (TK-0.20g, TK-0.45g, TK-0.69g, respectively). These peak ground acceleration levels were selected to represent moderate to severe ground motions. The specific record (downloaded from the PEER NGA Strong Motion Database, http://ngawest2.berkeley.edu/) is representative of the bedrock motion close to the Daikai Metro station, which collapsed during the 1995 earthquake [Iida 1996; Yoshida 1996; Power et al. 1996; Nakamura et al. 1996; Hashash 2001; Lanzano et al. 2008]. Figure 4b illustrates the elastic acceleration response spectra of the scaled TK records. In Fig. 4c, the normalised response spectra are compared to the Eurocode 8 (EC8) design spectra for $\xi = 5\%$, together with the free-field (FF) response spectra based on the FE analysis results (ground motions at 100m distance from the tunnel centreline) for $D_r = 60\%$ and $100\%$. The FF response spectra can be compared to the EC8 Ground type C design spectrum, given the relative densities considered ($v_{s,30} \approx 280 m/s > 180 m/s$). As shown in Fig. 4a, the selected seismic excitation contains a long-period directivity pulse, due to which the plateau of its response spectrum extends to larger periods than the EC8 Ground type C design spectrum.

### *2.5. Tunnel construction (volume loss)*

According to Mair and Taylor [1997], the volume loss during the open-face excavation process of the tunnel can be defined as follows:

$$V_L = \frac{V_{settlement}}{V_{tunnel}} = \frac{\sqrt{2\pi} i S_{V,\max}}{A_{tunnel}} \tag{4}$$

where: $V_L$ is the volume loss, $A_{tunnel}$ is the ideally excavated volume of the tunnel (or area per unit length for the 2D model considered here), $S_{V,\max}$ is the settlement at the ground surface above the tunnel crown, and $i = Kz_0$ is a parameter affecting the shape of the settlement trough (this is essentially the point of inflexion of the Gaussian-shaped settlement trough that forms above the tunnel centreline). $K$ is a parameter approximately equal to 0.35 for stiff sands [Mair & Taylor 1997; Bloodworth 2002; Dragojevic 2012; Zhou 2015; Paolilo 2015] and $z_0$ is the depth of the tunnel's geometric centre.

Many previous studies have considered the magnitude of volume loss during NATM construction and how these values affect the settlements above the tunnel. The range of volume loss recorded across various projects can reach up to $V_L = 3.5\%$ [e.g., Mair & Taylor 1997; Dimmock & Mair 2007; Marshall et al. 2012; Zhou 2015] for open-face tunnel excavation, though this is an extreme value. In this paper, it is considered that the reference tunnel has been constructed with realistic volume loss values (i.e. simulating construction-induced stress relief only) ranging from $V_L = 0\%$ to 2%.

In 2D plane strain analysis, the most commonly used methods to simulate volume loss are the load reduction method ($\beta$-method) and the stiffness reduction method ($\alpha$-method) [Panet 1978; Mödlhammer 2010; Masin 2011; Dragojevic 2012; Avgerinos et al. 2016]. The $\beta$-method is adopted and employed in two sequential analysis steps: (a) the soil inside the tunnel cavity is extracted and the surrounding soil is allowed to contract until reaching a target settlement, $S_{V,\max}$ (Eq. 4), which corresponds to the target volume loss; (b) the tunnel lining is introduced, accommodating the resulting deformations from the previous soil contraction. The $\beta$-

method is chosen since its application allows a more direct correlation of the volume loss with the target settlement in PLAXIS 2D than the α-method.

The pre-earthquake settlements above the tunnel centreline can be calculated as follows:

$$S_V^{pre-eq}(x) = S_{V,\max}^{pre-eq} e^{-\left(\frac{x}{\sqrt{2}i}\right)^2} \quad (5)$$

where $S_{V,\max}^{pre-eq}$ are the maximum pre-earthquake settlements above the tunnel centreline.

Figure 5a shows the effect of volume loss on pre-earthquake surface settlement troughs for the $D_r = 60\%; c' = 0kPa$ case as an example. Figures 5b and 5c present the maximum pre-earthquake settlement, $S_{V,\max}^{pre-eq}$, and $i^{pre-eq}/D$ values for the cases of $D_r = 100\%; c' = 0kPa$, $D_r = 60\%; c' = 0kPa$ and $D_r = 60\%; c' = 50kPa$ against the volume loss values. As expected, the maximum pre-earthquake settlements increase with the increase of $V_L$, while the $i^{pre-eq}/D$ slightly decreases in accordance with the observation of Marshall et al. [2012].

To validate the replication of appropriate initial conditions following the *β*-method, Table 2 compares the computed pre-earthquake maximum settlement, $S_{V,\max}^{pre-eq}$, with the results of Zhou et al. [2014] and Zhou [2015] for a tunnel with diameter, $D = 7.2m$, cover depth, $C^Z = 14.4m$, surrounded by sand with $D_r = 50\%$. Table 2 also compares the computed $i^{pre-eq}/D$ values with the results of Marshall et al. [2012] for a tunnel with diameter, $D = 6.15m$, cover depth, $C^M = 8.18m$, surrounded by sand with $D_r = 90\%$ and also with Zhou et al. [2014] as described above. The differences in the results are negligible confirming the validity of the adopted approach for simulating the post-construction, pre-earthquake ground conditions. Additional validation of similar (or equivalent) soil constitutive models capturing and simulating volume loss effects numerically can be found in Likitlersuang et al. [2014] and Zhang et al. [2016].

## 3. RESULTS

### *3.1. Accelerations*

Free-field (FF) conditions are assumed at 100 m distance from the tunnel centreline, where the effects of soil-structure interaction were observed to be negligible. The near-field (NF) is assumed above and below the tunnel following its centreline. Figure 6 presents the settlement at the ground surface above the tunnel crown, the free-field and near-field horizontal accelerations at the ground surface, $\ddot{u}_x$, and similar ground accelerations below the tunnel for both the FF and NF during the TK-0.2g excitation for $D_r = 60\%, c' = 0kPa, V_L = 0\%$. Some effect of the tunnel can be seen in Figs. 6b and 6c; more specifically, the tunnel seems to slightly affect the acceleration response at the ground surface above the centreline by increasing the peak ground acceleration compared to the FF (Fig. 6b). This observation will be highlighted further in Fig. 8, as it can have wider implications on the seismic resilience of infrastructure above the tunnel centreline and within an influence zone from the tunnel that is still an open research question.

Figure 7 shows the response spectra of the ground surface motions at NF and FF positions for the $D_r = 60\%; c' = 0kPa$ case subjected to TK-0.69g and TK-0.20g, with $V_L = 0\%$. In both cases, some slightly increased amplification (NF compared to FF) is observed for $0.8s < T_n < 2s$, and for $T_n < 0.3s$ in the case of TK-0.20g. This may be of importance for tall buildings and bridges, which are at this range of periods. For smaller periods, the ground motion is somewhat attenuated, especially in the case of severe ground motions (TK-0.69g). This suggests that the hazard posed to these structures would decrease (by up to 20% in this specific case).

The effect of soil properties on spectral amplification is further elucidated in Fig. 8 which presents the ratio of NF to FF response spectra, $S_{A,NF} / S_{A,FF}$ (i.e., amplification due to the presence of tunnel), for the different soil properties considered, and all 3 seismic motions. It is evident from Fig. 8 that low rise buildings ($0.2s \le T \le 0.4s$) are potentially more detrimentally affected than taller structures when

subjected to smaller intensity seismic motions, though this effect disappears for the largest motions. This can be important in the context of performance-based design [Bertero & Bertero 2002], where (repairable) structural damage is to be avoided in more frequent smaller earthquakes, but is not expected to alter the vulnerability of such a class of structures in larger motions when life-safety is the performance requirement. In combination, Figs. 7 and 8 demonstrate that the construction of a new tunnel may affect the seismic actions acting on above-ground structures, something that may have consequences on the design of new structures and on the seismic vulnerability of existing ones.

Figure 9a presents the NF and FF peak ground acceleration (PGA) profile with depth $z$. Evidently, as the PGA increases the acceleration field in the vicinity of the tunnel ($z \approx 18m - 26m$) increasingly diverges from the FF values. This suggests that it may be inappropriate to use FF motions from site-response analyses in tunnel structural response models in design, as this may lead to a significant underestimation of the actions on the tunnel lining, particularly for the most damaging motions. Figure 9b illustrates the FF amplification ratios, $S_{FF}$, based on PGA values in NF and FF rather than spectral values, for $D_r = 60\%,100\%$, $V_L = 0\%, 1\%, 2\%$, and $c' = 0kPa, 50kPa$. These values represent the 'ground type' amplification factors used in Eurocode 8 and other codes. The $S_{FF}$ values decrease with increasing PGA of the bedrock motion, in agreement with previous centrifuge and numerical data from Knappett et al. (2015), which is associated with increasing elastic soil response in larger motions, which limits potential site amplification. However, it can be seen that in most cases volume loss and soil relative density have only a very limited effect on this parameter compared to the presence of cohesion which reduces amplification substantially. The $S_{FF}$ follow the EC8 amplification factor for Ground type C.

### *3.2. Lining forces*

Figure 10 plots the maximum lining forces for the largest seismic excitation (TK-0.69g), including the circumferential forces $N$ (Fig. 10a), the shear forces $V$ (Fig. 10b), and the bending moments $M$ (Fig. 10c). The results are compared for a rough, $\mu = 1$, and a finite stiffness and strength, $\mu = 0.6$, interface between the tunnel and the surrounding soil (both in parallel and normal directions to the interface), representing potential upper and lower bounds for a sprayed-concrete tunnel lining in accordance with Uesugi et al. (1990). This $\mu$ coefficient defines a new elastic modulus and strength for the interface based on the soil properties, in order for potential slipping or gapping to take place along the tangential and perpendicular direction respectively [PLAXIS 2D Reference Manual, 2016]. For example, the elastic modulus along the perpendicular, $E_{int}$, and the tangential direction, $G_{int}$, become:

$$E_{int} = 2G_{int}\frac{1-\nu_i}{1-2\nu_i}$$
$$G_{int} = \mu^2 G_{soil} \leq G_{soil}, \nu_i = 0.45 \quad (6)$$

The bending moment (sign) plotting convention follows the deformed shape of the lining, thus the negative moments signify tension on the internal surfaces of the tunnel. Following this convention, the term "sagging" refers to negative moments of the arch section and positive moments of the flat section. Accordingly, the term "hogging" bending moments is used to represent the positive bending moments of the arch section and the negative bending moments of the flat section (close to the springing), respectively. It is evident that the lining forces, particularly the circumferential ones, are lower for $\mu = 0.6$. This suggests that it may be conservative to assume a rough interface to determine the seismically-induced actions within the tunnel lining for structural detailing. Another interesting observation is that the maximum hoop forces and "sagging" bending moments do not occur at the tunnel crown, but rather at a distance from it following the damage patterns of Lanzano et al. [2008] and Wang [1993]. The maximum shear forces and "hogging" bending moments occur at the tunnel springing ("elephant's foot") where the circular part/arch section meets the flat section representing stiff supports for both the arch and the flat sections.

Figure 11 compares the maximum values of the lining forces for different relative soil densities, $D_r = 60\%,100\%$, between the perfectly excavated tunnel, $V_L = 0\%,$ and increasing volume losses ($V_L = 1\%, 2\%$). In all cases examined, the magnitude of the maximum lining forces increases with increasing PGA. Furthermore, the increase of volume loss results to a significant reduction of the lining forces because of the initial contraction of the soil close to the tunnel; an observation which is more obvious for small to moderate PGA values. However, the effect of volume loss reduces with increasing PGA as the initial conditions (volume loss) do not dominate the dynamic response during a very strong excitation. In addition, lower density soil results in slightly higher lining forces than the higher density soil in most cases; a result that is highlighted with increasing volume loss. These results suggest that for the purposes of tunnel structural design, analyses considering a perfect tunnel ($V_L$ = 0%) should provide an upper-bound to the likely structural actions induced.

Another interesting finding is that the results follow the design strategy of the geometrically composite tunnel section; that is, the arch section "translates" the external soil pressure more effectively into circumferential forces/stresses rather than shear forces, whereas the flat section, which resembles the typical behaviour of a beam, results in substantial shear forces compared to the arch section. The latter emphasizes the importance of selecting an appropriate structural geometry for the seismic design of such tunnels. Figure 12 extends the results of Fig. 10 as it presents the maximum lining forces for relative soil densities, $D_r = 60\%,100\%$, accounting both for a rough, $\mu = 1$, and a finite strength, $\mu = 0.6$, interface between the tunnel and the surrounding soil. As expected, the maximum lining forces in the case of the $\mu = 0.6$ interface are smaller than in the case of the rough interface for all cases examined, with a few exceptions (mostly in "sagging" moments). The greatest differences are associated with the circumferential and shear forces rather than the bending moments. In these plots the effect of the composite structural geometry is further highlighted by the pronounced differences of the circumferential and shear forces between the arch and the flat sections of the tunnel.

Figure 13 illustrates the effect of apparent cohesion (comparing $c' = 0kPa$ with $c' = 50kPa$) on the maximum lining forces for relative soil density, $D_r = 60\%$, and $V_L = 0\%, 1\%, 2\%$ in the case of. The addition of cohesion significantly reduces the maximum lining forces, especially combined with a volume loss increase. This is because for the same volume loss, the tunnel contracts more in the presence of cohesion. However, this outcome becomes less significant with the increase of PGA, since initial conditions' (volume loss) effect on the response becomes more negligible for severe ground excitations. In combination with the previous results, the design assumption of a rough interface and no cohesion will result in conservative estimates of lining forces, and this should also be reasonable in terms of ground motion amplification at the ground surface (see Figs. 8 and 9).

### *3.3. Induced Settlements*

Figure 14a illustrates the pre- and post-earthquake settlement trough above the tunnel:

$$S_V(x) = \left(S_{V,\max} - S_{V,FF}\right) e^{-\left(\frac{x-b}{\sqrt{2}i}\right)^2} \tag{6}$$

where $S_V(x)$ is the settlements at any point $x$, $S_{V,\max}$ represents the maximum settlement in the trough, $S_{V,FF}$ the free-field settlements (which are zero before the seismic excitation), $i$ the settlement trough shape parameter (defined by the inflexion point on the trough), and $b$ is a new parameter that defines the observed offset of the location of the post-earthquake maximum settlement from the tunnel centreline ( $b = 0$ for pre-earthquake settlements). Figure 14b presents an example case for $D_r = 60\%$ subjected to the TK-0.2g motion, and the Gaussian curve fits to the FE analysis data for both pre- (star markers) and post-earthquake cases (circle markers). As expected, the Gaussian fitting index in the case of the post-earthquake

settlements is not as close as in the case of the pre-earthquake settlements ($R^2_{pre-eq.} > R^2_{post-eq.}$), but still represents a good approximation of the shape of the trough.

Figure 15 presents the maximum post-earthquake free-field (FF) settlement values, $S_{FF}$, in function of PGA. It is clear that for very large PGA, the $S_{FF}$ increases disproportionally due to the increasingly non-linear inelastic response of the soil for larger ground motions. Interestingly, Fig. 16a shows that the differential settlement trough, $S_{V,\max} - S_{V,FF}$, is not necessarily dependent on PGA. The larger intensity ground motions (larger PGA) are affecting a wider area, and are therefore inducing larger volumetric changes on the soil body. As a result, while the volumetric strain may increase with the increase of PGA, the same does not apply to the differential settlements. Furthermore, Fig. 16a shows that as the volume loss during the construction of the tunnel increases, the differential settlements increase as well. This is a result of the partial void collapse (application of the $\beta$-method), due to which the soil moves closer to yielding before the seismic excitation.

Additionally, Fig. 16b shows that the settlement trough shape, $i/D$, becomes increasingly sensitive to the soil properties and volume loss for the more severe ground motions, while, for moderate intensity ground motions it seems rather insensitive. However, the cohesion plays a significant role on the curvature parameter, $i/D$, as the curvature of the settlement trough does not seem to get affected significantly from PGA. Furthermore, the increase of the volume loss tends to decrease the $i/D$ values resulting in narrower post-earthquake settlement troughs, especially for large PGA.

Finally, Fig. 16c introduces parameter $b/D$ (the offset of the maximum post-earthquake settlement from the tunnel centreline), which seems to alternate from left to right of the tunnel centreline with increasing PGA, resulting in the maximum post-earthquake settlement not being necessarily above the tunnel crown: depending on PGA, it may be located up to $\pm 0.4D$ away from the tunnel centreline. Figure 16c illustrates a very interesting aspect of post-earthquake settlements: high intensity ground motions might result in non-

symmetric settlements, as the $b / D$ ratio gets finite values different than zero (pre-earthquake settlements). This observation may lead to a change in the area on the ground surface where the hazard from the differential settlements is higher than above the tunnel's centreline ($b / D = 0$). However, cohesive soils (triangular markers) tend to settle more symmetrically, even for severe excitations compared to sandy soils. The above-mentioned results showcase that predicting post-earthquake settlements can be a quite challenging numerical task as they can be affected by numerous parameters.

## 4. CONCLUSION

In this paper, the seismic behaviour of horseshoe-shaped tunnels in coarse-grained sandy soils has been investigated using nonlinear finite element modelling, with a particular focus on the effect of volume loss during tunnel construction. The constitutive model used for the analyses had been previously validated against centrifuge model test data for wished-in-place tunnels, and was further validated here in terms of capturing pre-earthquake settlement troughs due to construction-induced volume loss against other previously published centrifuge data. A parametric study has been conducted, varying soil density, interface properties, cohesion, and volume loss during tunnel construction. Nevertheless, it should be noted that the results presented herein are limited by the tunnel geometry, the model domain/boundary conditions and the chosen excitations considered.

It was shown that the presence of the tunnel and the effects of its construction leads to amplification of the ground motion and to an increase of the seismic hazard posed to low-rise structures ($0.2s \le T \le 0.4s$) by up to 50% in smaller motions compared to the free-field response that would be obtained from a non-linear site-amplification study. However, this effect reduces with increasing PGA (towards a maximum of 10% amplification) due to nonlinear soil response. In general, the tunnel presence may increase the seismic hazard for taller or more flexible structures ($T \ge 0.8s$, e.g. taller buildings and bridges) by up to 20%

(largely insensitive to ground conditions). While the increase of cohesion leads to increased amplification, the consideration of volume loss does not lead to an appreciable change of ground surface accelerations.

The tunnel lining forces were shown to be strongly affected by its geometry; the arch section tends to more effectively convert the external pressures from the surrounding soil into circumferential stresses compared to the flat bottom section that (resembling a typical beam) tends to develop much higher transverse shear forces. The maximum circumferential forces and sagging bending moments during earthquake shaking are not located at the tunnel's centreline. The presence of a finite-strength interface, $\mu = 0.6$, tends to reduce the lining forces (as expected) particularly in terms of the hoop stresses. The consideration of volume loss reduces the co-seismic internal forces as well, but this effect decreases with increasing PGA. Furthermore, the presence of apparent cohesion reduces the lining forces significantly, especially in combination with volume loss (as a result of the greater contraction associated with the same target volume loss values in a cohesionless soil). Therefore, the most conservative design assumptions for the purposes of structural detailing consist of a rough interface, zero cohesion, and negligible volume loss (i.e., an ideally-excavated tunnel).

Finally, the paper examined the effect of the aforementioned parameters on the pre- and post-earthquake settlements at the ground surface. It was observed that the maximum post-earthquake settlements tend to increase with PGA; this is principally due to larger volumetric settlements in the free-field, though the differential component of the settlement trough is magnified in the strongest earthquakes. The increase of PGA tends to create wider post-earthquake settlement troughs, potentially spreading the zone of damage at the ground surface, although volume loss results in narrower troughs which may at least partially compensate. Volume loss increases the pre-earthquake maximum settlements but reduces the component induced by the earthquake. The addition of cohesion results in smaller settlement values with narrower troughs. Post-earthquake settlement troughs were observed to be asymmetric and an additional parameter ($b/D$) was introduced into conventional Gaussian models to capture this. For the ground motions considered, the maximum settlement was observed to be located up to b = $\pm 0.4D$ from the tunnel centreline

depending on the shaking intensity meaning that the expected zone of damaged structures due to differential settlement may not be precisely indicated by those structures that were most significantly deformed during tunnel construction.

## ACKNOWLEDGEMENTS

This work was supported by the Newton Fund: EPSRC, UK & CONICYT Chile: Shaking tunnel vision. Joint project led by University of Leeds EP/N03435X/1.

## REFERENCES

1. Al-Defae AH, Caucis K and Knappett JA [2013] "Aftershocks and the whole-life seismic performance of granular slopes". Geotechnique **63(14)**: 1230–1244.
2. Amorosi A and Boldini D [2009]. Numerical modelling of the transverse dynamic behaviour of circular tunnels in clayey soils. Soil Dynamics and Earthquake Engineering **29(6)**: 1059–72.
3. Amorosi A, Boldini D and Gaetano E [2010]. Parametric study on seismic ground response by finite element modelling. Computers and Geotechnics, **37**: 515-528.
4. Amorosi, A, Boldini, D and Falcone, G, [2014]. Numerical prediction of tunnel performance during centrifuge dynamic tests. Acta Geotechnica, **9**: 581-596.
5. Amorosi A, Boldini D and Di Lernia, A [2017]. Dynamic soil-structure interaction: A three-dimensional numerical approach and its application to the Lotung case study. Computers and Geotechnics, **90**:34-54.
6. Anastasopulos I, Gerolymos N, Drosos V, Kourkoulis R, Georgakakos T, and Gazetas G [2007]. Nonlinear response of deep immersed tunnel to strong seismic shaking. Journal of Geotechnical and Environmental Engineering **133(9)**: 1067-1090.

7. Anastasopulos I, Gerolymos N, Drosos V, Georgakakos T, Kourkoulis R, and Gazetas G [2008]. Nonlinear response of deep immersed tunnel to strong seismic shaking. Bulletin of Earthquake Engineering **6**: 213-239.
8. Anastasopoulos I and Gazetas G [2010]. Analysis of cut-and-cover tunnels against large tectonic deformation. Bulletin of Earthquake Engineering **8**: 283-307.
9. Aoyagi T [1995]. Representing Settlement for Soft Ground Tunnelling. PhD Thesis, MIT.
10. Argyroudis S, Tsinidis G, Gatti F, and Pitilakis K [2017]. Effects of SSI and lining corrosion on the seismic vulnerability of shallow circular tunnels. Soil Dynamics and Earthquake Engineering **98**: 244-256.
11. Avgerinos V, Potts DM, Standing JR [2016]. The use of kinematic hardening models for predicting tunnelling-induced ground movement in London Clay. Geotechnique **66(2)**: 106-120.
12. Bilotta E, Lanzano G, Madabhushi SPG, Silvestri F [2014]. A numerical Round Robin on tunnels under seismic actions. Acta Geotechnica **9**: 563-579.
13. Benz T [2006]. Small-strain stiffness of soils and its numerical consequences. PhD thesis, University of Stuttgart, Germany.
14. Bertero RD, Bertero VV [2002]. Performance-based seismic engineering: the need for a reliable conceptual comprehensive approach. Earthquake Engineering and Structural Dynamics **31**: 627-652. DOI: 10.1002/eqe.146
15. Bloodworth AG [2002]. Three-Dimensional analysis of tunnelling effects on structures to develop design methods. PhD Thesis, University of Oxford.
16. Bransby MF, Brown MJ, Knappett JA, Hudacsek P, Morgan N, Cathie D, Maconochie A, Yun G, Ripley AG, Brown N and Egborge R [2011]. Vertical capacity of grillage foundations in sand. Canadian Geotechnical Journal **48(8)**: 1246–1265. DOI: 10.1139/t11-040
17. CEN [1998] EN 1998- 5:2004. Eurocode 8: design of structures for earthquake resistance – Part 5: Foundations, retaining structures and geotechnical aspects. Brussels: European Committee for Standardization; Belgium.

18. Cilingir U, Madabhushi SPG [2011]. A model study on the effects of input motion on the seismic behaviour of tunnels. Soil Dynamics and Earthquake Engineering **31**:452–462.
19. Cilingir U, Madabhushi SPG [2011]. Effect of depth on the seismic response of circular tunnels. Canadian Geotechnical Journal **48(1)**:117–27.
20. Computers and Structures [2006]. *SAP 2000 Documentation*, University of California, Berkeley, USA.
21. Dimmock PS and Mair RJ [2007]. Volume loss experienced on open-face london clay tunnels. Geotechnical Engineering , *ICE, GEI* **160**: 3-11.
22. Dowding CH and Rozen A [1978]. Damage to rock tunnels from earthquake shaking. Journal of Geotechnical Engineering **104(GT2)**:175–191.
23. Dragojevic SM [2012]. Analysis of ground settlement caused by tunnel construction. Gradevinar **64(7)**: 573-581.
24. Hardin BO and Drnevich VP [1972]. Shear modulus and damping in soils: design equations and curves. Journal of Soil Mechanics and Foundations Division, ASCE **98(SM7)**: 667–692.
25. Hashash YMA, Hook JJ, Schmidt and Yao JI-C [2001]. Seismic design and analysis of underground structures. Tunnel and Underground Space Technology **16(2)**:247–293.
26. Iida H, Hiroto T, Yoshida N and Iwafuji M [1996]. Damage to Daikai subway station. *Special issue on geotechnical aspects of the January 17 1995 Hyogoken–Nanbu earthquake. Soils Foundation* 283–300.
27. Kawashima K [1999]. Seismic design of underground structures in soft ground, a review. *Proceedings of the International Symposium on Tunnelling in Difficult Ground Conditions*. Tokyo, Japan.
28. Knappett JA, Madden P, and Caucis K [2015]. Seismic structure-soil-structure interaction between pairs of adjacent building structures. Geotechnique **65(5)**: 429-441.
29. Kontoe S and Zdravkovic L, Potts DM and Menkiti CO [2008]. Case study on seismic tunnel response. Canadian Geotechnical Journal **45**: 1743-1764.

30. Kontoe S, Zdravkovic L, Potts DM, and Menkiti CO [2011]. On the relative merits of simple and advanced constitutive models in dynamic analysis of tunnels. Geotechnique **61(10)**: 815-829.
31. Kontoe S, Zdravkovic L, Potts DM and Menkiti CO [2008]. Case study on the seismic tunnel response. Canadian Geotechnical Journal **45(12)**: 1743-1764.
32. Kwok AOL, Stewart JP, Hashash YMA, Matasovic N, Pyke R, and Wang Z [2007]. Use of exact solutions of wave propagation problems to guide implementation of nonlinear seismic ground response analysis procedures. Journal of Geotechnical and Geoenvironmental Engineering **133(11)**: 1385–98.
33. Lanzano G, Bilotta E, Russo G and Silvestri F [2015]. Experimental and numerical study on circular tunnels under seismic loading. European Journal of Environmental and Civil Engineering, **19(5)**: 539-563.
34. Lanzano G, Bilotta E and Russo G [2008]. Strategies for reduction of the seismic risk; Tunnels under seismic loading: a review of damage case histories and protection methods. *Mitigation of the Earthquake Effects in Towns and in Industrial Regional Districts (MEETING)*, 65-74.
35. Lauder K, Brown MJ, Bransby MF and Boyes S [2013]. The influence of incorporating a forecutter on the performance of offshore pipeline ploughs. Applied Ocean Research Journal **39**: 121-130. DOI: 10.1016/j.apor.2012.11.001.
36. Liang, T, Knappett, J.A., Leung, A, and Bengough, G, [2019]. Modelling the seismic performance of root-reinforced slopes using the finite-element method. Geotechnique, doi.org/10.1680/jgeot.17.P.128
37. Likitlersuang, S, Surarak, C, Suwansawat, S, Wanatowski, D, Oh, E, and Balasubramaniam, A, [2014]. Simplified finite-element modelling for tunnelling-induced settlements. Geotechnical Research, 1(4): 133-152.
38. Lysmer J and Kuhlmeyer RL [1969]. Finite dynamic model for infinite media. Journal of Engineering Mechanics Division, ASCE **95(4)**: 859–887.

39. Mair RJ and Taylor RN [1997]. Bored tunnelling in the urban environment. *In 14th International conference on soil mechanics and foundation engineering*, pp. 2353–2385.
40. Marshall A, Farrell R, Klar A and Mair R [2012]. Tunnels in sands: the effect of size, depth and volume loss on greenfield displacements. Geotechnique **2(5)**: 385–399.
41. Mödlhammer H [2010]. *Numerical methods for tunnelling using ABAQUS and investigation of long-time-effects of the shotcrete shell and its impact on the combined support system*. M.Sc. Thesis, MIT.
42. Nakamura S, Yoshida N, Iwatate T [1996]. Damage to Daikai subway station during the 1995 Hyogoken–Nambu earthquake and its investigation. *Japan Society of Civil Engineers, Committee of Earthquake Engineering*, pp 287–295.
43. O' Rourke TD, Goh SH, Menkiti CO and Mair RJ [2001]. Highway tunnel performance during the 1999 Düzce earthquake. *In: Proceedings of the 15th International Conference on Soil Mechanics and Geotechnical Engineering*, August 27–31, Istanbul.
44. Panet M [1978]. Stability Analysis of a Tunnel driven in a rock mass in tracking account of the post-failure behavior. Rock Mechanics, **8(1)**: 209-223.
45. Paolillo A [2015]. Ground movement induced by tunnelling. *Universita Degli Studi Di Napoli Federico II*.
46. PEER NGA Strong Motion Database. See http://ngawest2.berkeley.edu/ .
47. Brinkgreve RBJ and Vermeer PA [1998]. Plaxis manual. *Version, 7*, 5-1.
48. Power MS, Rosidi D, Kaneshiro J [1996]. *Vol. III Strawman: screening, evaluation, and retrofit design of tunnels*. Report Draft. National Center for Earthquake Engineering Research, Buffalo, New York.
49. Santos JA and Correia AG [2001]. Reference threshold shear strain of soil: its application to obtain a unique strain-dependent shear modulus curve for soil. *Proceedings of the 15th international conference on soil mechanics and geotechnical engineering*, Istanbul, Turkey, vol. 1, pp. 267–270.

50. Schanz T, Vermeer PA and Bonnier PG [1999]. *The hardening soil model: formulation and verification*. In Beyond 2000 in computation geotechnics (ed. RBJ Brinkgreve), pp. 281–290. Rotterdam, the Netherlands: Balkema.
51. Smith IM, Griffiths DV [1982]. *Programming the Finite Element Method*. John Wiley & Sons, Chisester, U.K., 2nd edition.
52. Smith CC and Gilbert M [2007]. Application of discontinuity layout optimization to plane plasticity problems. Proceedings of the Royal Society London A **463(2086)**: 2461–2484.
53. Svoboda T, and Masin D [2011]. *Comparison of displacement field predicted by 2D and 3D finite element modelling of shallow NATM tunnels in clays*. Charles University in Prague.
54. Tsinidis G, Pitilakis K, Madabhushi G and Heron C [2015]. Dynamic response of flexible square tunnels: centrifuge testing and validation of existing design methodologies. Geotechnique **65(5)**: 401–417.
55. Tsinidis G, Pitilakis K and Anagnostopoulos C [2016a]. Circular tunnels in sand: dynamic response and efficiency of seismic analysis methods at extreme lining flexibilities. Bulletin of Earthquake Engineering **14**: 2903–29.
56. Tsinidis G, Pitilakis K and Madabhushi G [2016b]. On the dynamic response of square tunnels in sand. Engineering Structures **125**: 419–437.
57. Ueng TS, Lin ML, and Chen MH [2001]. Some geotechnical aspects of 1999 Chi-Chi, Taiwan earthquake. *Proceedings of the Fourth International Conference on Recent Advances in Geotechnical Earthquake Engineering and Soil Dynamics*. SPL-10.1, 5 p.1-5
58. Uesugi M, Kishida H, and Uchikawa Y [1990]. Friction between sand and concrete under monotonic and repeated loading. Soils and Foundations, **30(1)**: 115-128.
59. Vassiliou MF and Makris N [2011]. Estimating time scales and length scales in pulse like earthquake acceleration records with wavelet analysis. Bulletin of the Seismological Society of America **101(2)**: 596–618.

60. Wang JN [1993]. *Seismic design of tunnels: A state-of-the-art approach*. Monograph 7. New York: Parsons, Brinckerhoff, Quade and Douglas, Inc.
61. Yoshida N [2009]. Damage to subway station during the 1995 Hyogoken-Nambu (Kobe) earthquake. *In T. Kokusho (Ed.), Earthquake geotechnical case histories for performance-based design*. Tokyo: CRC Press, pp. 373–389.
62. Yu H, Yuan Y, Qiao Z, Gu Y, Yan Z and Li X. [2013]. Seismic analysis of a long tunnel based on multiscale method. Engineering Structures **49**: 572-587.
63. Yu H, Yuan Y, Xu G, Su Q, Yan X and Li C. [2018]. Multi-point shaking table test for long tunnels subjected to non-uniform seismic loadings – part II: Application to HZM immersed tunnel. Soil Dynamics and Earthquake Engineering **108**: 187-195.
64. Yu H, Zhang Z, Chen J, Bobet A, Zhao M and Yuan Y. [2018]. Analytical solution for longitudinal seismic response of tunnel liners with sharp stiffness transition. Tunnelling and Underground Technology **77**: 103-114.
65. Yu H, Cai C, Bobet A, Zhao X and Yuan Y. [2019]. Analytical solution for longitudinal bending stiffness of shied tunnels. Tunnelling and Underground Technology **83**:27-34.
66. Yuan Y, Yu H, Li C, Yan X and Yuan J. [2018]. Multi-point shaking table test for long tunnels subjected to non-uniform seismic loadings – Part I: Theory and validation. Soil Dynamics and Earthquake Engineering **108**: 177-186.
67. Zerwer A, Cascante G and Hutchinson J [2002]. Parameter estimation in finite element simulations of Rayleigh waves. Journal of Geotechnical and Geoenvironmental Engineering **128(3)**: 250–261.
68. Zhang J, Yuan Y and Yu H. [2019a]. Shaking table tests on discrepant responses of shaft-tunnel junction in soft soil under transverse excitations. Soil Dynamics and Earthquake Engineering **120**: 345-359.
69. Zhang J, Yuan Y, Bao Z, Yu H, Bilotta E. [2019b]. Shaking table tests on the intersection of cross passage and twin tunnels. Soil Dynamics and Earthquake Engineering, **124**: 136-150.

70. Zhang, Z.X., Liu, C, Huang, X, Kwok, C.Y., and Teng, L, (2016). Three-dimensional finite-element analysis on ground response during twin-tunnel construction using the URUP method. Tunelling and Underground Space Technology, 58: 133-146.
71. Zhou B, Marhall AM and Yum H-S [2014]. The Effect of Relative Density on Settlements above Tunnels in Sands. *Geotechnical Special Publication: Tunnelling and Underground Construction GSP 242@ ASCE*, 96-105.
72. Zhou B [2015]. *Tunnelling-induced Ground Displacements in Sand*. PhD Thesis, University of Nottingham.

**APPENDIX**

The same numerical model for $D_r = 60\%; c' = 0kPa; V_L = 2\%$ has been used with both (i) absorbent viscous and (ii) tied-node side boundaries in order to reveal any differences between the two modelling approaches. Fig. A1 shows the comparison between the two different cases for: (a) horizontal displacement, (b) horizontal acceleration and (c) vertical displacement (settlement) at the ground surface above the tunnel crown, when the tunnel is excited by TK-0.20g. The errors between the peak values for horizontal displacements and accelerations and the last values for settlements is presented in Table A1 accordingly. It is evident from the results that the discrepancies between the two modelling approaches are not significant or critical for the purpose of the paper. A similar result has been shown in Liang et al. [2019].

**Table A1**. Error percentages of the differences between the peak values of (a) horizontal displacements; (b) horizontal accelerations and last values of (c) vertical displacements (settlements) at the ground surface above the tunnel crown, when the tunnel is excited by TK-0.20g.

| Horizontal displacements | Horizontal accelerations | Vertical displacements |
|---|---|---|

| | | |
|---|---|---|
| **0.36%** | **7.77%** | **4.40%** |

(a)

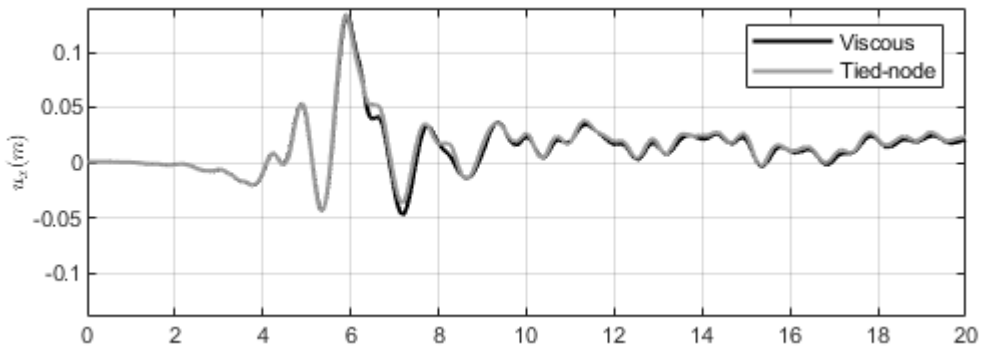


(b)

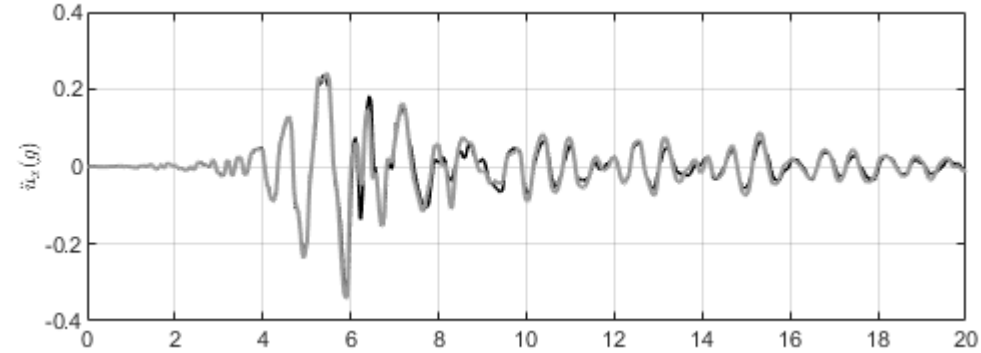


(c)

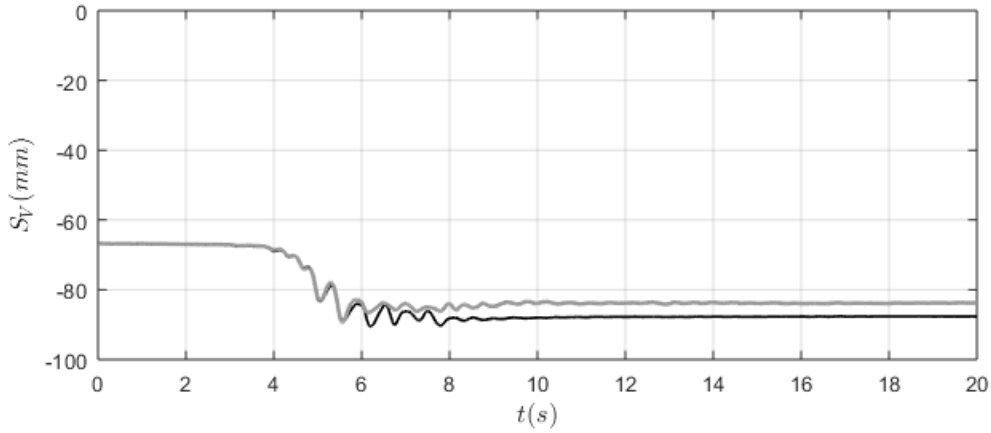

**Figure A1**. Comparison between the tunnel model with absorbent viscous (black) and tied-node (grey) side boundaries in terms of (a) horizontal displacements; (b) horizontal accelerations and (c) vertical displacements (settlements) at the ground surface above the tunnel crown, when the tunnel is excited by TK-0.20g.

**Tables**

**Table 1.** Model parameters for HST95 sand of relative density $D_r = 60\%$ and $100\,\%$ .

| **HST95 Parameters** | $D_r = 60\%$ | $D_r = 100\%$ |
|---|---|---|
| unit weight, $\gamma_d\,(kN/m^3)$ | 16.30 | 17.50 |
| saturated unit weight, $\gamma_{sat}\,(kN/m^3)$ | 19.88 | 20.60 |
| secant stiffness in drained triaxial test $E_{50}\,(kPa)$ | 44,025 | 56,525 |
| tangent stiffness for primary oedometer loading $E_{oed}\,(kPa)$ | 35,220 | 42,370 |
| unloading-reloading stiffness, $E_{ur}\,(kPa)$ | 105,600 | 135,600 |
| small-strain stiffness, $G_0^{ref}\,(kPa)$ | 118,800 | 138,800 |
| shear strain, $\gamma_{s,0.7}$ | $1.7\times10^{-4}$ | $2.4\times10^{-4}$ |
| peak friction angle, $\varphi'(^o)$ | 41.00 | 49.00 |
| dilatancy angle, $\psi(^o)$ | 11.20 | 21.60 |
| apparent cohesion, $c'(kPa)$ | 0 or 50 | 0 |
| $m$ | 0.54 | 0.50 |

**Table 2**. Comparison of pre-earthquake maximum settlements, $S_{V,\max}^{pre-eq}\,(mm)$ , and $i^{pre-eq}/D$ values with Marshall et al. (2012), Zhou et al. (2014), and Zhou (2015) for different volume loss levels.

| **Max. pre-earthquake settlements** | **Volume loss** |
|---|---|

| $S_{V,\max}^{pre-eq}(mm)$ | $V_L = 1\%$ | $V_L = 2\%$ | $V_L = 3\%$ |
|---|---|---|---|
| This study | 25.8 | 51.6 | 77.3 |
| Zhou at al. (2014) | | | 68 |
| Zhou (2015) | 28 | 52 | |
| $i^{pre-eq} / D$ | $V_L = 1\%$ | | $V_L = 3\%$ |
| This study | 0.81 | | 1.13 |
| Marshall et al. (2012) | 0.96 | | |
| Zhou et al. (2014) | | | 1.02 |

**Figures**

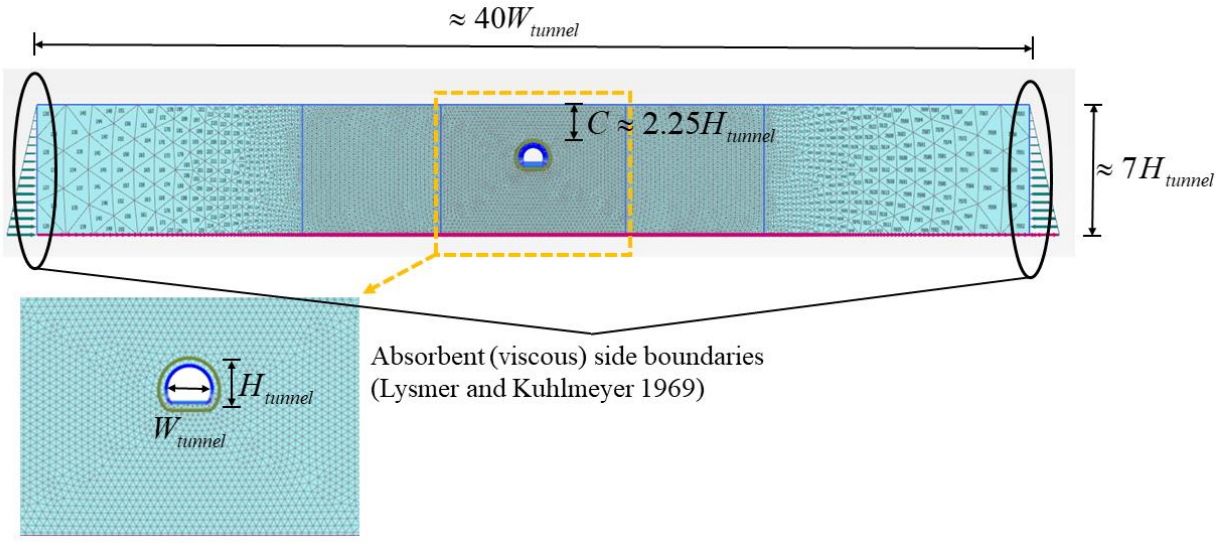


**Figure 1**. Finite element mesh of the "horseshoe"-shaped tunnel, inspired from sprayed-concrete tunnels in Chile.

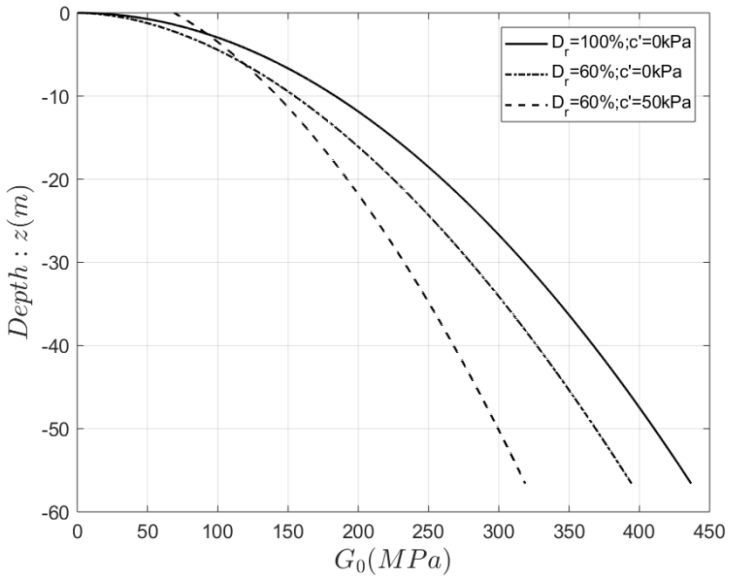


**Figure 2**. Distribution of $G_0$ with depth, $z$ , for the cases of $D_r = 100\%; c' = 0kPa$, $D_r = 60\%; c' = 0kPa$ and $D_r = 60\%; c' = 50kPa$.

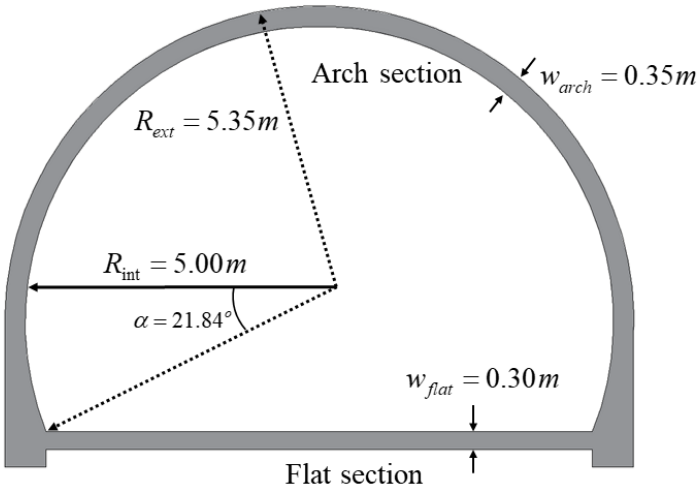


**Figure 3.** Reinforced concrete "horseshoe" tunnel section used in this study, inspired by Metro tunnels in Santiago, Chile.

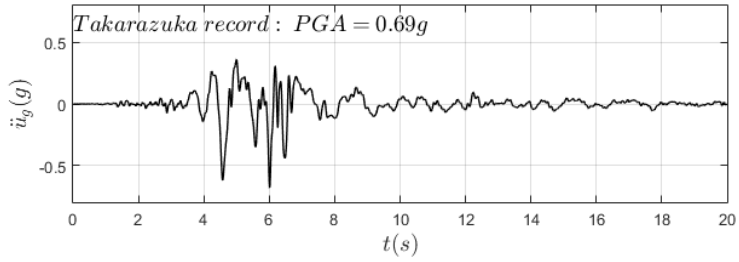
$Takarazuka\ record:\ PGA = 0.69g$
0.5
0
-0.5
$\ddot{u}_g(g)$
0
2
4
6
8
10
12
14
16
18
20
$t(s)$

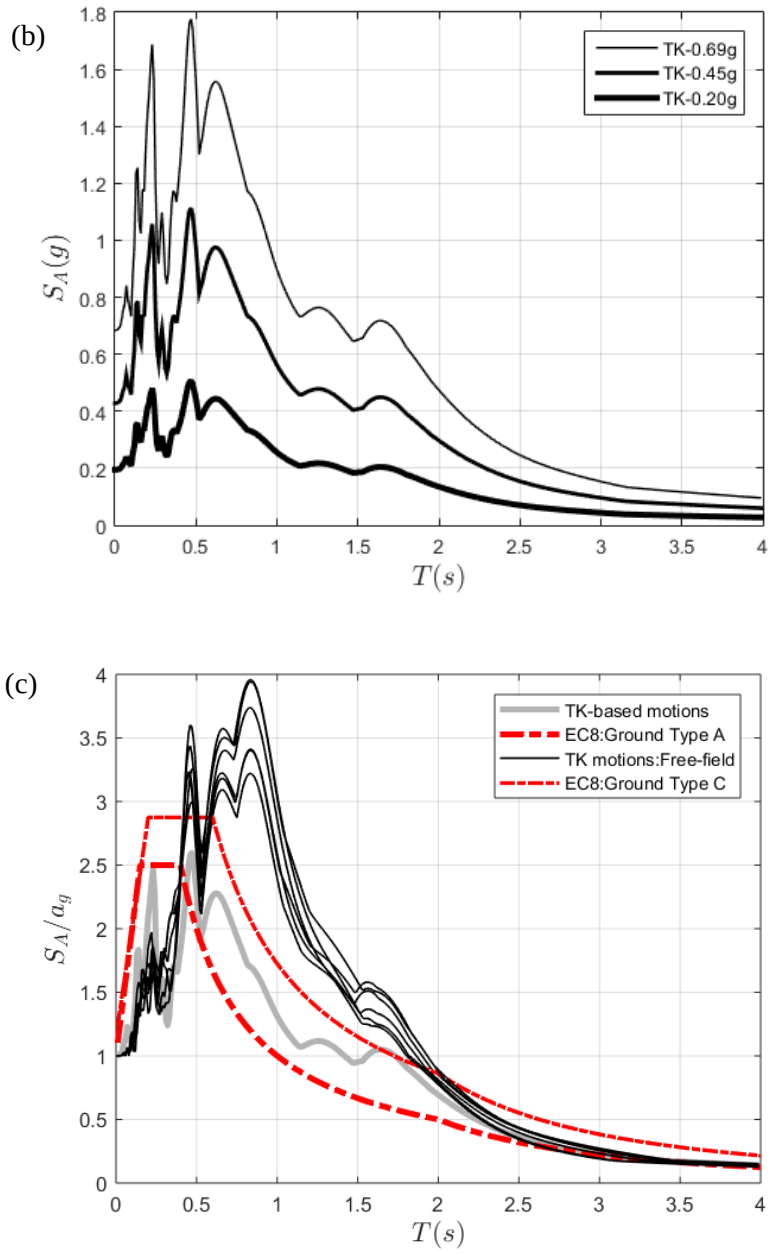


**Figure 4.** (a) The Takarazuka record from the 1995 Kobe earthquake, used as seismic excitation (scaled at $a_g = 0.20g$, $0.45g$ and $0.69g$); (b) response spectra of the three scaled motions for $\xi$ = 5% damping; (c) comparison between the normalised response spectra of the scaled input (bedrock) records and the free-field response from FE analysis with the Eurocode 8 (EC8) design spectra for Ground type A and C.

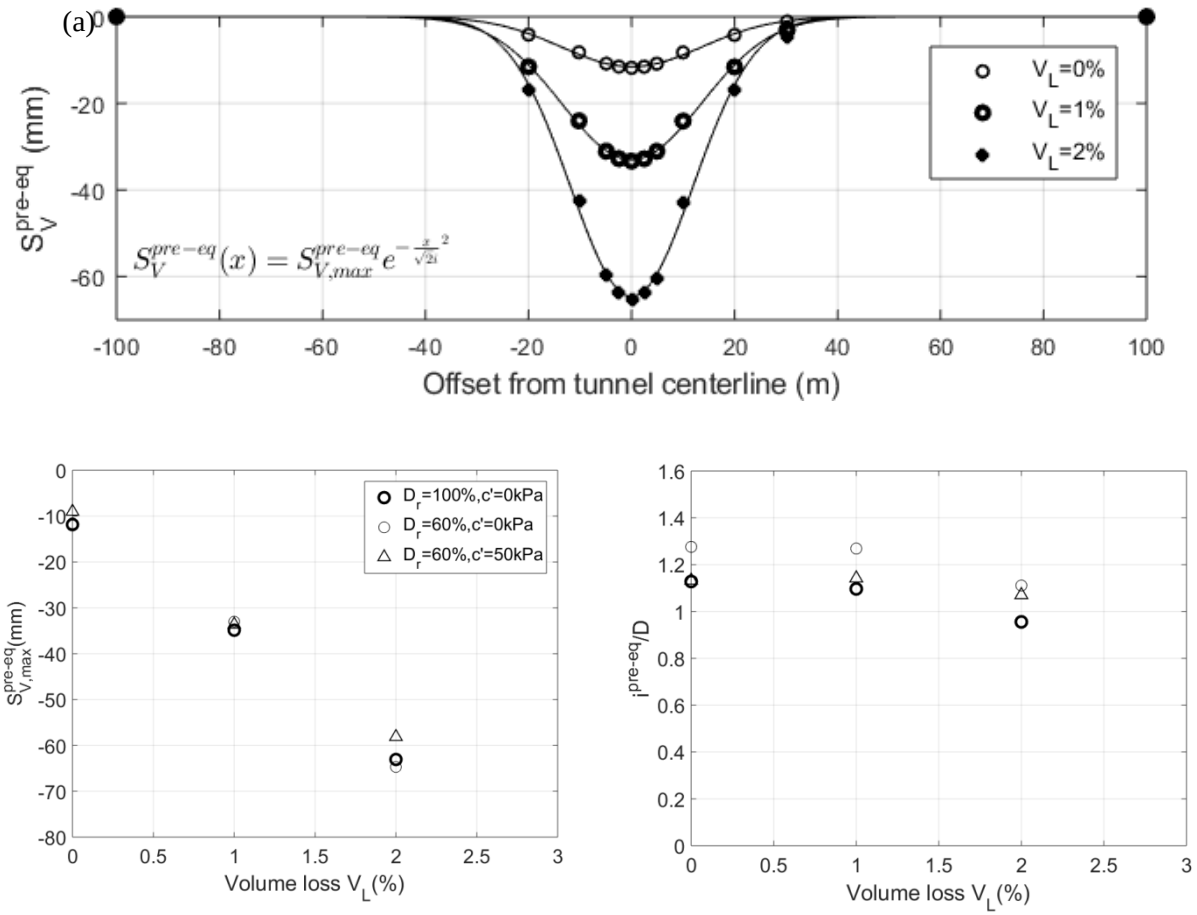


**Figure 5**. (a) Pre-earthquake settlement troughs for $D_r = 60\%; c' = 0kPa$ ; (b) maximum pre-earthquake settlements, $S_{V,\max}^{pre-eq}$ and (c) $i^{pre-eq} / D$ values for $D_r = 100\%; c' = 0kPa$, $D_r = 60\%; c' = 0kPa$ and $D_r = 60\%; c' = 50kPa$ against volume loss, $V_L = 0\%, 1\%, 2\%$, accordingly.

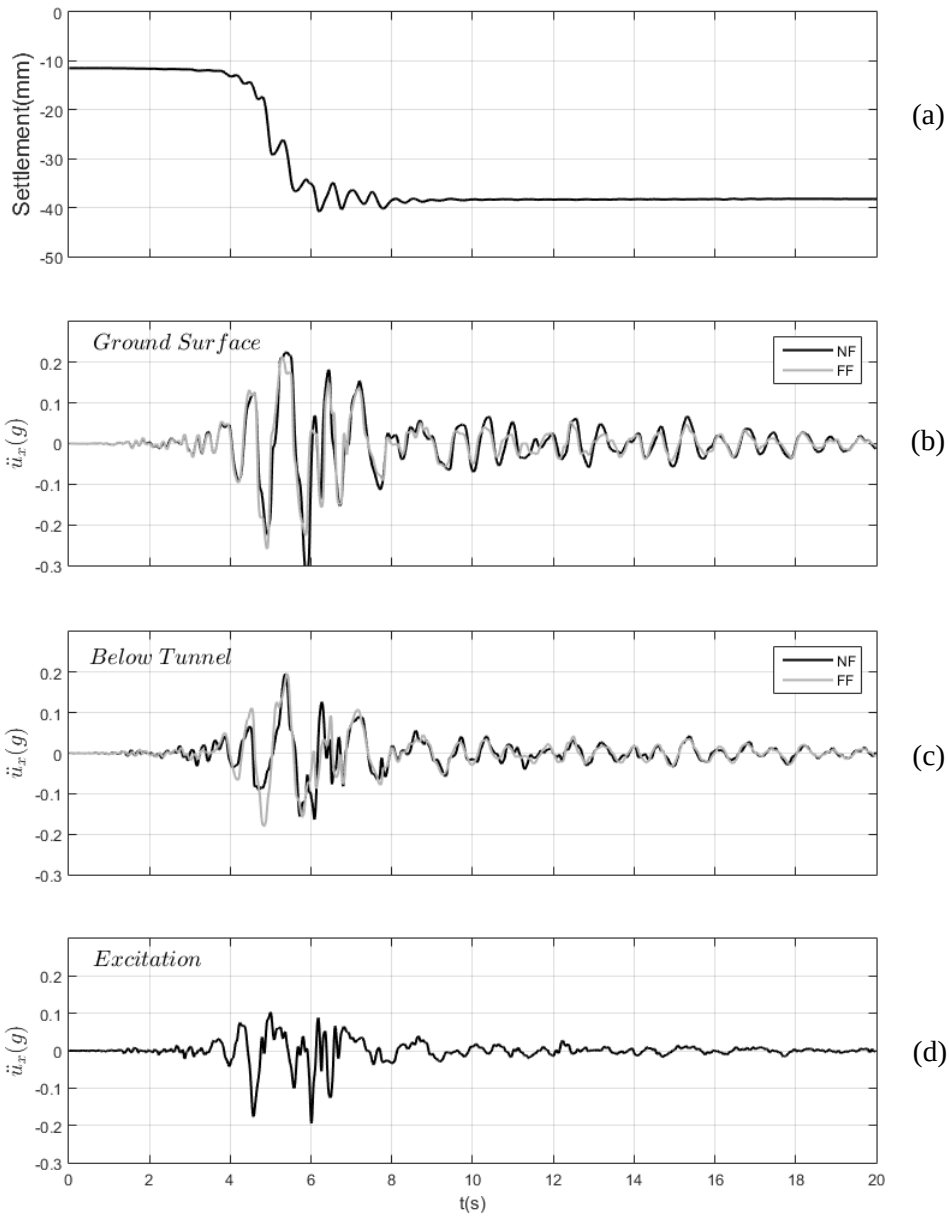


**Figure 6**. Tunnel subjected to TK-0.2g seismic excitation, $D_r = 60\%$, $c' = 0kPa$, $V_L = 0\%$. Time histories of: (a) settlement at the ground surface above the tunnel crown; (b) near-field (NF) and free-field (FF) horizontal acceleration, $\ddot{u}_x$, at the ground surface above the tunnel crown; (c) near-field (NF) and free-field (FF) horizontal acceleration below the tunnel; and (d) seismic excitation.

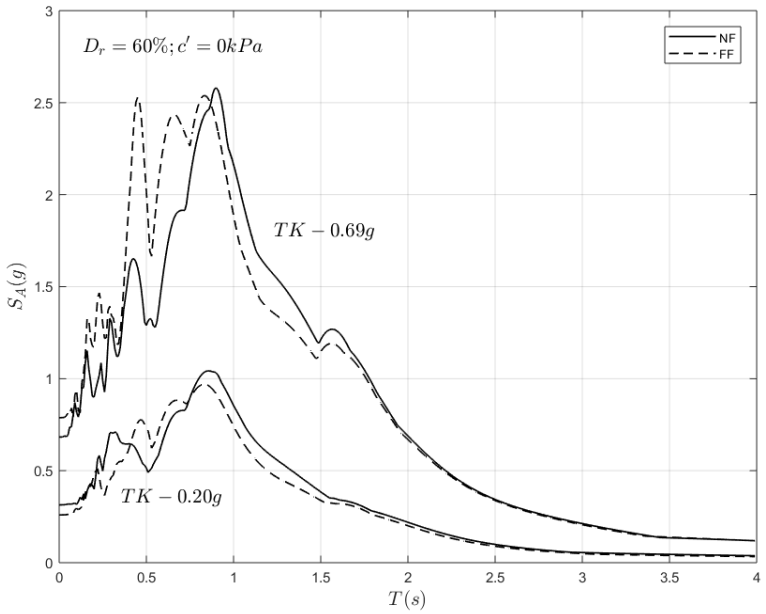


**Figure 7**. Response spectra of the NF (above the tunnel centreline) and FF (ground surface) for the case of $D_r = 60\%; c' = 0kPa$ , subjected to TK-0.20g and TK-0.69g.

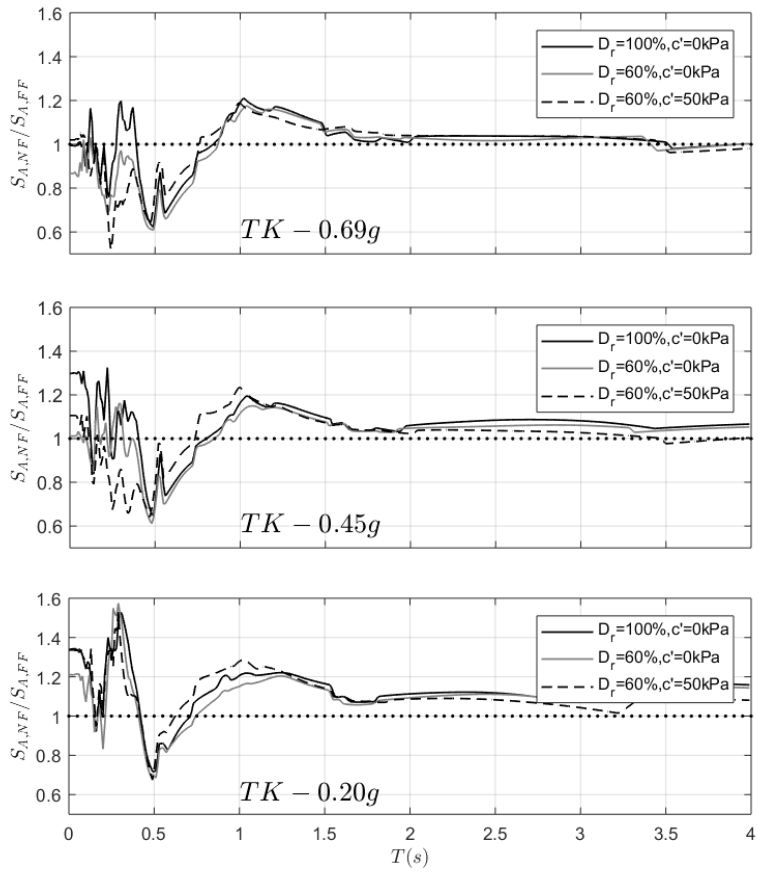


(a)

(b)

(c)

**Figure 8.** Near-field (NF) over free-field (FF) acceleration response ratios, $S_{A,NF} / S_{A,FF}$ for three different soil properties ( $D_r = 100\%; c' = 0kPa$, $D_r = 60\%; c' = 0kPa$ and $D_r = 60\%; c' = 50kPa$ ) subjected to: (a) TK-0.69g; (b) TK-045g; and (c) TK-0.20g.

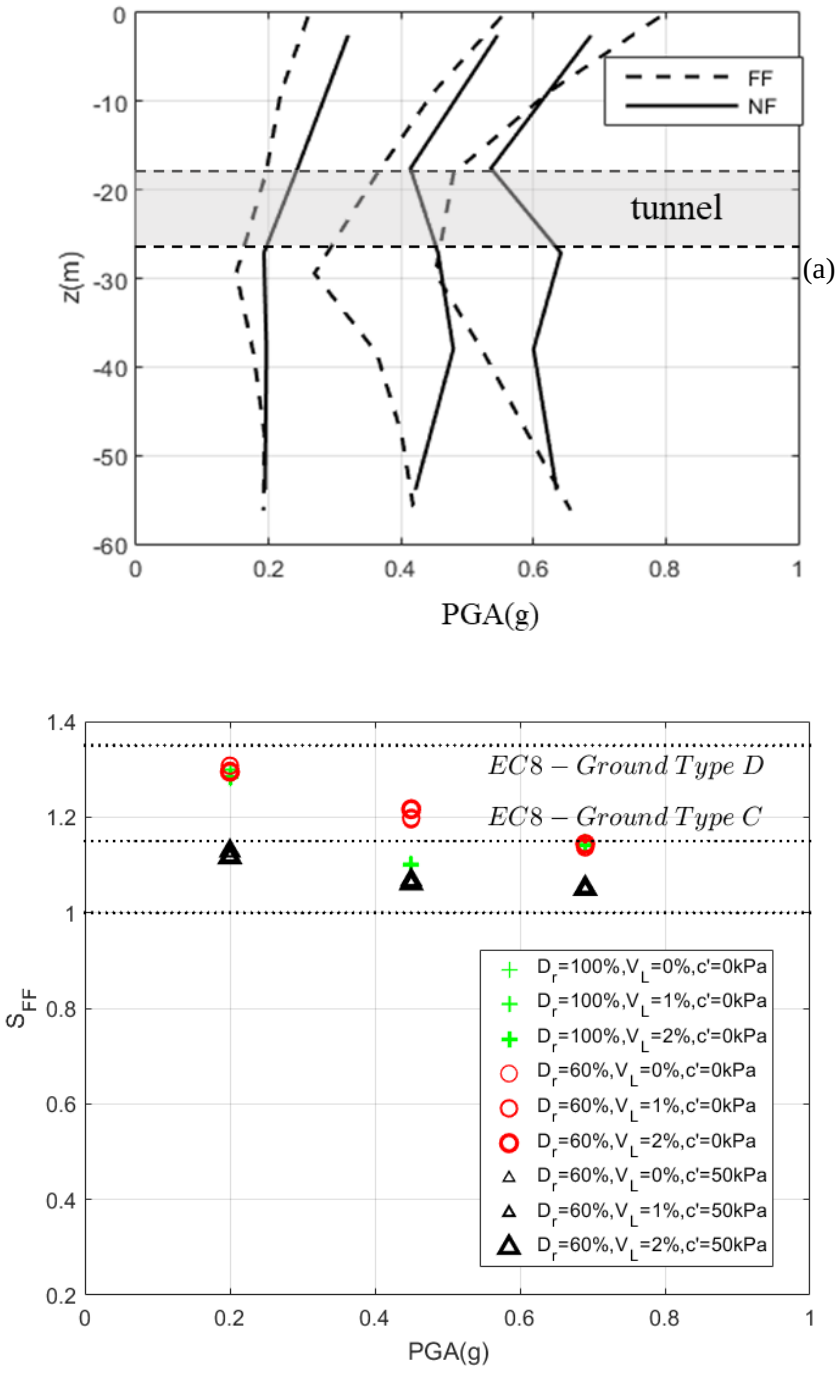


**Figure 9**. (a) Near-field (NF) and free-field (FF) peak acceleration profile with depth $z$ ; (b) FF amplification factors, $S_{FF}$ , varying with PGA for $D_r = 60\%,100\%$ , $V_L = 0\%, 1\%, 2\%$ and $c' = 0kPa, 50kPa$ .

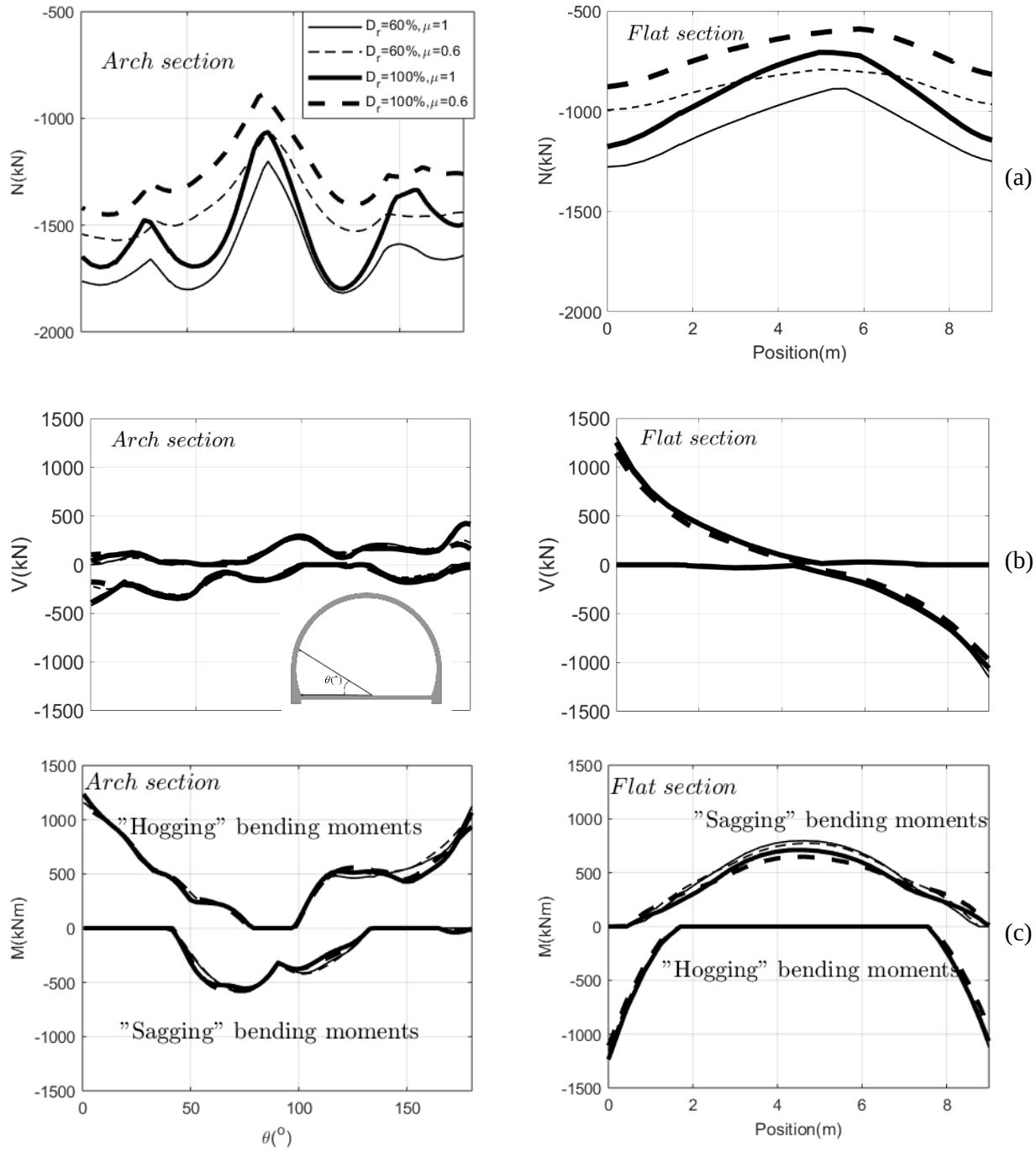


**Figure 10**. The effect of soil and interface properties on tunnel lining forces: (a) circumferential forces; (b) shear forces; and (c) bending moments. For the arch section the results are plotted with the angle $\theta$; for the feat secion with position. TK-0.69g excitation, $D_r = 60\%,100\%$, rough and limited slip interface.

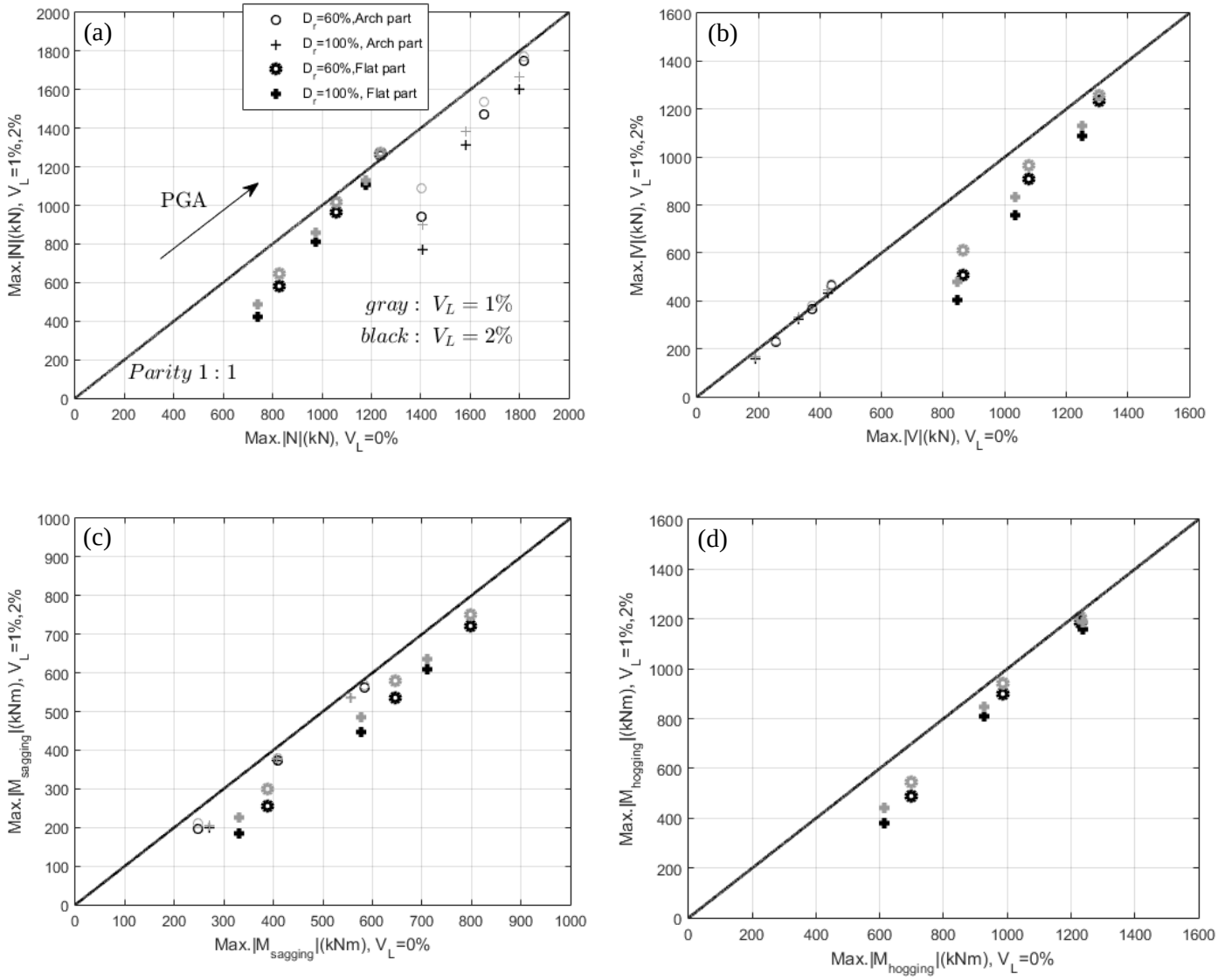


**Figure 11.** The effect of volume loss on tunnel lining forces: (a) maximum circumferential force *N*; (b) maximum shear force *V*; and (c) maximum "sagging" bending moment $M_{sagging}$; and (d) maximum "hogging" bending moment $M_{hogging}$, for a rough interface between tunnel and the surrounding soil.

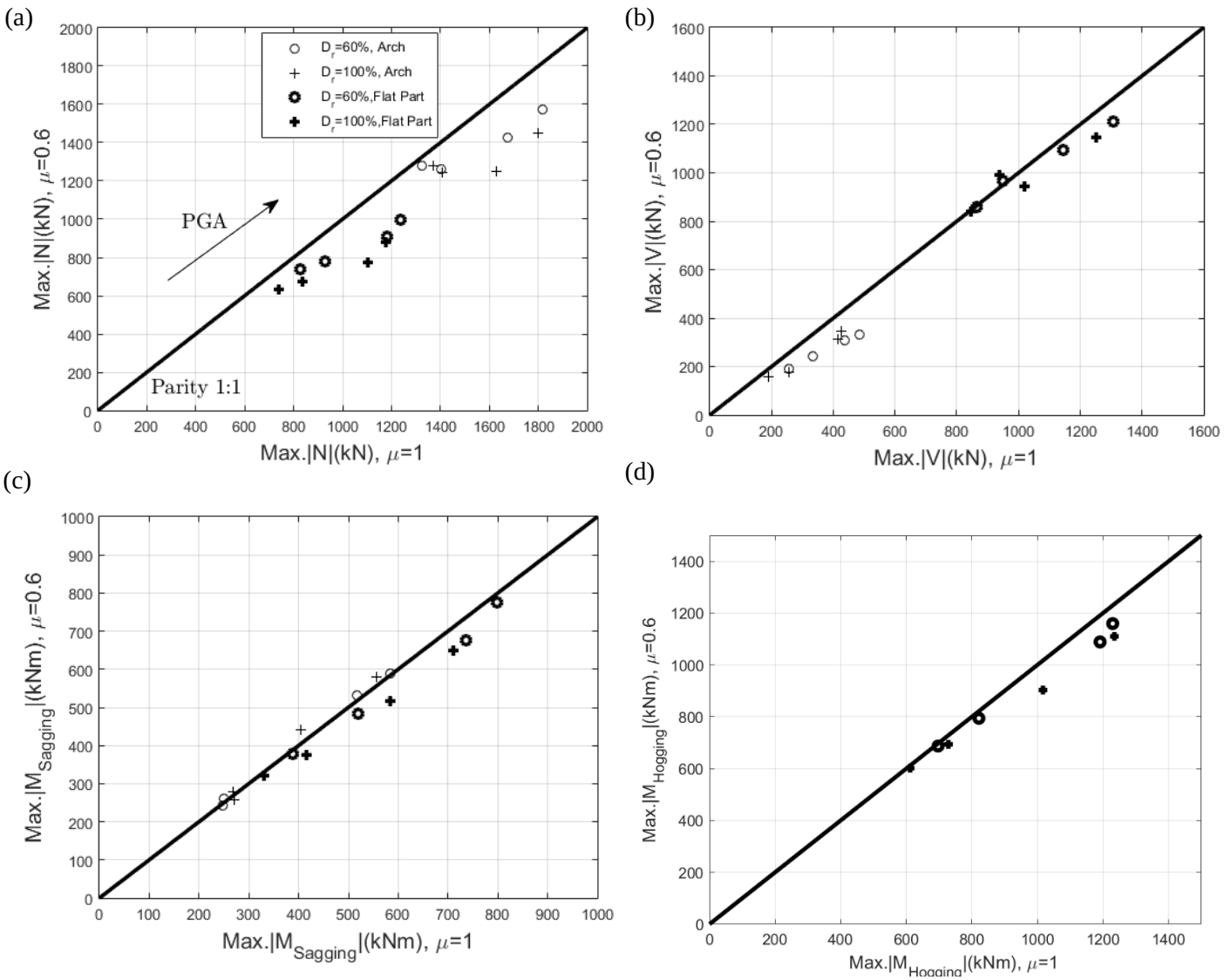


**Figure 12.** The effect of interface properties on tunnel lining forces: (a) maximum circumferential force *N*; (b) maximum shear force *V*; and (c) maximum "sagging" bending moment $M_{sagging}$; and (d) maximum "hogging" bending moment $M_{hogging}$.

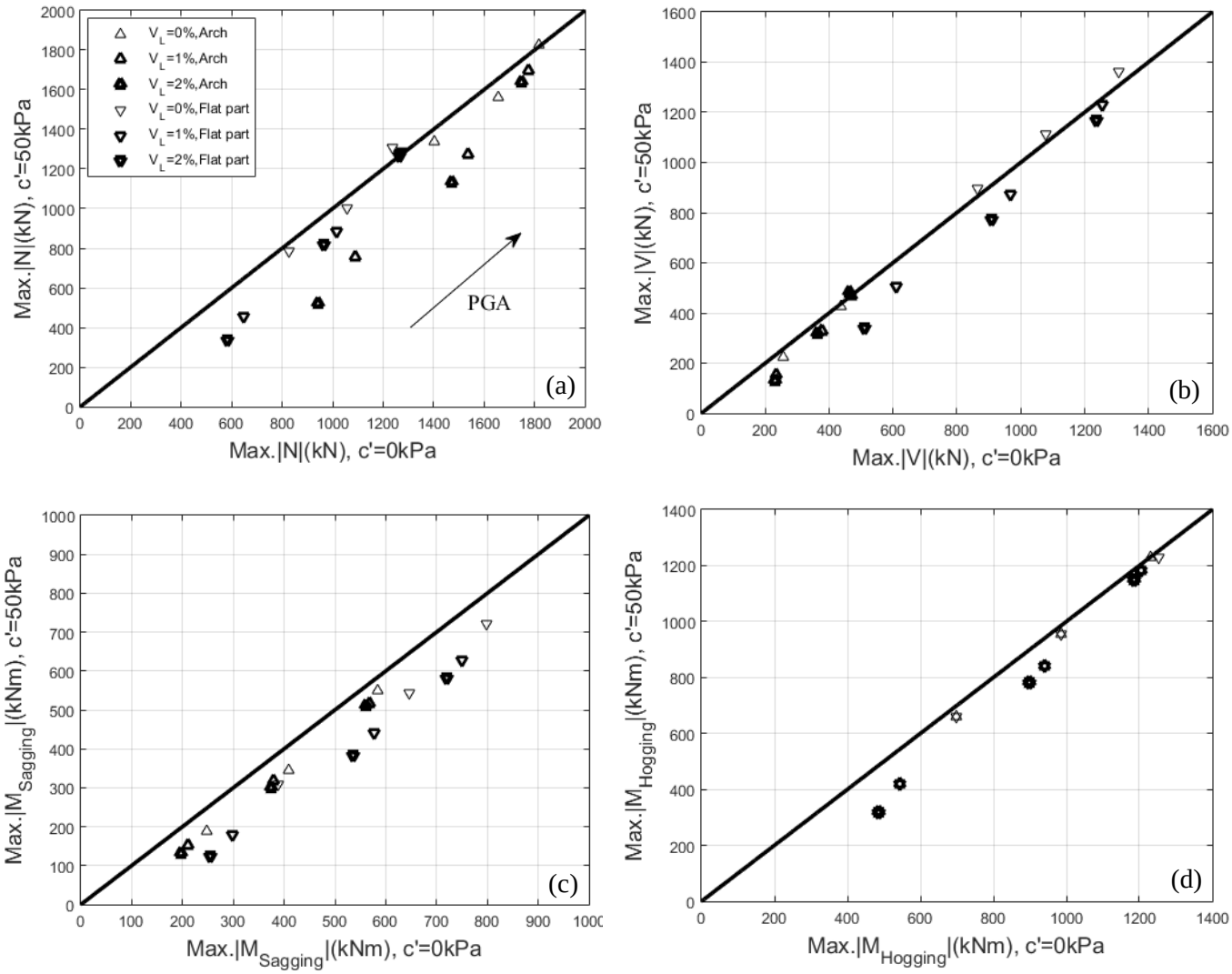


**Figure 13.** The effect of cohesion on tunnel lining forces: (a) maximum circumferential force *N*; (b) maximum shear force *V*; and (c) maximum "sagging" bending moment $M_{sagging}$; and (d) maximum "hogging" bending moment $M_{hogging}$.

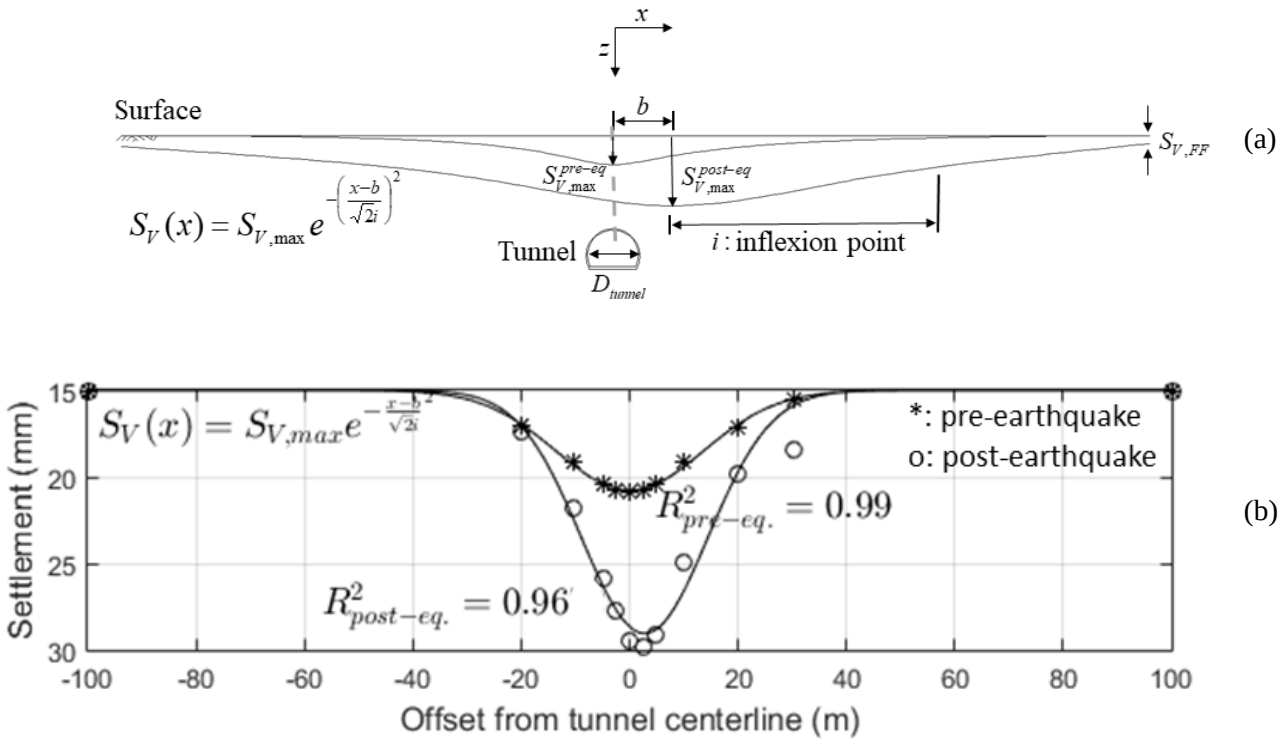


**Figure 14.** (a) Pre- and post-earthquake settlement trough above the tunnel; (b) Gaussian curve fitting on the pre- and post-earthquake data at the ground surface above the tunnel (VL = 0%, TK-0.2g).

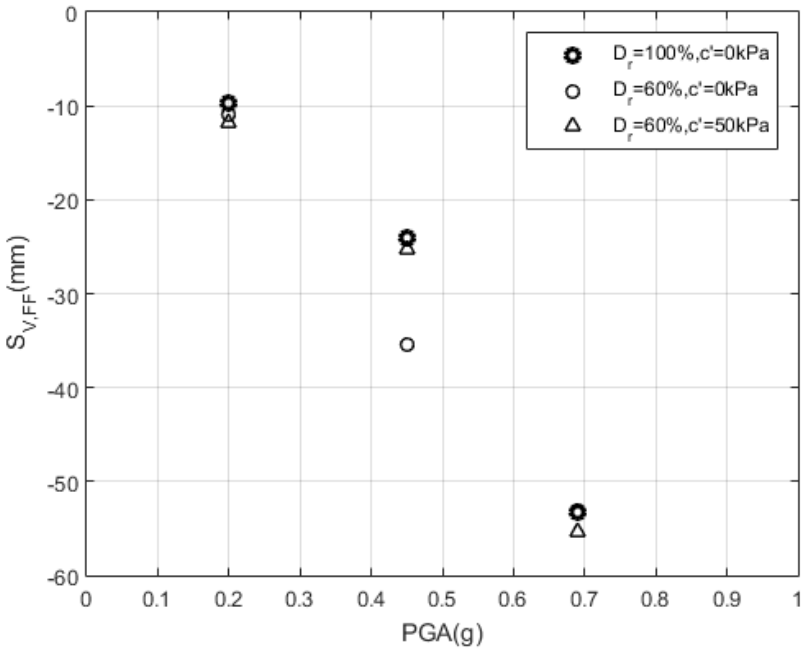


**Figure 15.** Maximum post-earthquake free-field (FF) settlement $S_{V,FF}$ .

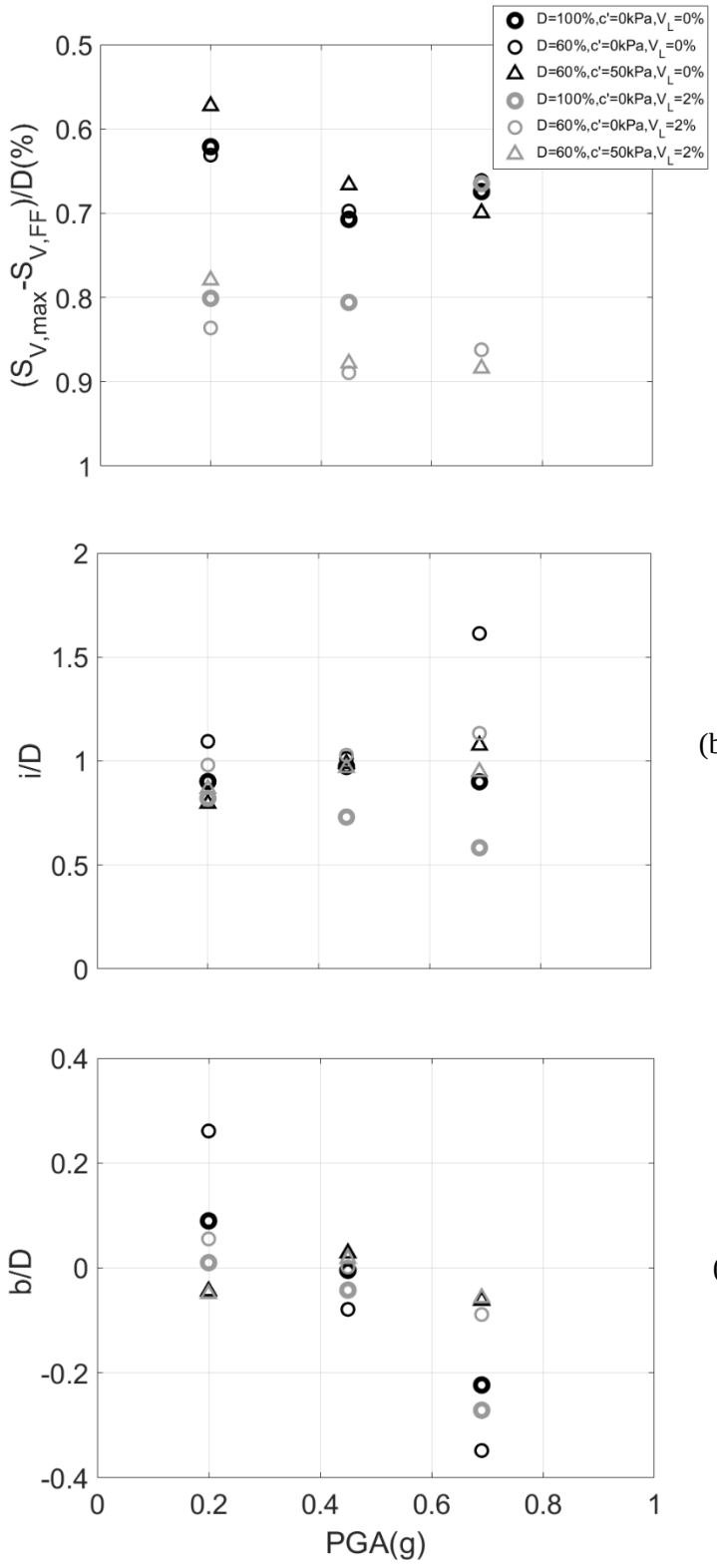


**Figure 16.** Post-earthquake settlements in function of PGA: (a) normalized maximum settlements, $(S_{V,\max} - S_{V,FF})/D$; (b) $i/D$; and (c) $b/D$.